JOURNAL OF AIRCRAFT
Vol. 44, No. 3, May–June 2007

Drag Prediction in Transitional Flow over Airfoils

Wassim A. Basha* and Wahid S. Ghaly†
Concordia University, Montreal, Quebec H3G 1M8, Canada

DOI: 10.2514/1.22939

When simulating the flow over airfoils at relatively low Reynolds numbers, transition from laminar to turbulent flow plays an important role in determining the flow features and in quantifying the airfoil performance such as lift and drag. Hence a proper modeling of transition, including both the onset and extent, will lead to a more accurate drag prediction. The current paper presents a transition model that combines existing methods for predicting the onset and extent of transition, which are compatible with the Spalart–Allmaras turbulence model (Spalart, P. R., and Allmaras, S. R., "One Equation Turbulence Model for Aerodynamic Flows," AIAA Paper 92-0439, Jan. 1992), in which the flow is simulated using Fluent, a commercial computational fluid dynamics package. The transition onset prediction uses the Cebeci and Smith correlation (Cebeci, T., and Smith, A. M. O., "CS Method for Turbulent Boundary Layers," *Analysis of Turbulent Boundary Layers*, 1st ed., Academic Press, New York, 1974, pp. 329–384), which is based on the Michel method, for steady incompressible two-dimensional flow, whereas the extent of transition is quantified by developing a model for the intermittency function. The proposed transition model is implemented into Fluent; it is then used in simulating transitional flow in different well-documented experimental cases that cover single-element and two-element airfoils under different freestream conditions. Given the experimental data, the results obtained with the developed transition model reflect a consistent and significant improvement in drag prediction, when compared with the drag predicted using a fully turbulent flow simulation.

Nomenclature

C	=	model parameter
C_μ	=	model constant, $C_\mu = 0.11$
d	=	distance to the nearest wall
Re_c	=	Reynolds number based on the chord length, $=uc/\nu$
Re_x	=	Reynolds number based on local distance, $=u_e x/\nu$
Re_θ	=	Reynolds number based on momentum thickness, $=u_e\theta/\nu$
u	=	velocity
u_e	=	velocity at the edge of the boundary layer
x_i	=	point of instability to the Tollmien–Schlichting
x_t	=	transition onset
y^+	=	viscous sublayer Reynolds number, $=\rho u_\tau y_p/\mu$
Γ	=	transition intermittency function
Γ_b	=	normal-distance-dependent intermittency function
Γ_x	=	surface-distance-dependent intermittency function
θ	=	momentum thickness
μ	=	viscosity
ν	=	kinematic viscosity
Ω	=	vorticity vector magnitude

Subscripts

i	=	point of instability to the Tollmien–Schlichting
L	=	laminar
t	=	transition onset/turbulent flow
tr	=	transition onset
∞	=	freestream conditions

Presented as Paper 248 at the 44th AIAA Aerospace Sciences Meeting and Exhibit, Reno, Nevada, 9–12 January 2006; received 22 May 2006; revision received 9 September 2006; accepted for publication 14 September 2006. Copyright © 2006 by Basha and Ghaly. Published by the American Institute of Aeronautics and Astronautics, Inc., with permission. Copies of this paper may be made for personal or internal use, on condition that the copier pay the $10.00 per-copy fee to the Copyright Clearance Center, Inc., 222 Rosewood Drive, Danvers, MA 01923; include the code 0021-8669/07 $10.00 in correspondence with the CCC.

*Research Assistant, Concordia University, Mechanical and Industrial Engineering Department, EV 14-115, 1455 de Maisonneuve West. AIAA Student Member.

†Associate Professor, Concordia University, Mechanical and Industrial Engineering Department, EV 4-151, 1455 de Maisonneuve West. AIAA Senior Member.

I. Introduction

WITH the maturity of computational fluid dynamics (CFD) methods and the ever increasing computing power, engineers are spending more time using CFD tools to design, analyze, and predict the aircraft aerodynamic performance. Given that wind-tunnel testing is time consuming, very expensive, and elaborate, designers are also using CFD to reduce to a minimum the number of tests that need to be performed so as to validate a given design, hence reducing the cost of any new product. However, and despite of all the advances that have been made in the CFD discipline, there is still the need for improvement, particularly when it comes to accurately predicting the aerodynamic drag. That is why accurate drag prediction is an important area of active research.

What makes accurately predicting drag so important is its sensitivity to all the details of the CFD simulation and its influence on the aerodynamic performance of flying objects, airplanes in particular. As an example of drag effect on aircraft design, a reduction of one drag count ($\Delta C_D = 10^{-4}$) on a subsonic civil transport airplane means about 200 lb (one person) more in payload [1]. Another study carried out on the Lockheed C-5 airplane showed that one drag count at cruise conditions (0.4% of the total drag on the aircraft) is equivalent to about 1000 lb in load [1]. Thus it is crucial that the drag values predicted from CFD flow simulations would be as close as possible to the actual in-flight values to reflect the actual performance of the aircraft and thus supply a more reliable performance prediction.

Drag over a wing can be divided into three major components: viscous, induced, and wave drag. Induced drag is generated by the downwash velocity induced by the wing tip vortices; wave drag is a result of the shock waves generated in transonic flows. As for the viscous drag, it is mostly generated by skin friction and thus it is directly related to viscous flow behavior [1]. Induced and wave drag are generated by normal forces and thus they can be well predicted using Euler equations simulations provided that the viscous effects are confined to a thin layer near the wall. On the other hand, viscous drag can only be predicted by solving the Navier–Stokes equations due to the fact that they are generated by tangential forces [1]. Because induced drag is inherently a three-dimensional effect and wave drag is inherently a transonic effect, this study focuses on the two-dimensional, incompressible ($M_\infty \leq 0.4$) transitional flow over airfoils so as to focus attention on the viscous drag component.

During CFD-based drag evaluation, several critical factors have to be considered. Those factors range from geometry fidelity, mesh

quality, flow solver, convergence level, laminar-to-turbulent flow transition, turbulence model, and drag evaluation method [2]. The involvement of all these elements, whether in a positive or negative way, makes it more difficult to accurately estimate the drag using CFD.

The focus of this work is on modeling the boundary-layer flow transition from laminar to turbulent flow. This model predicts the transition onset and its extent. It is implemented into the Spalart–Allmaras model available in the commercial CFD code, Fluent, and is assessed for a single- and a two-element airfoil in two-dimensional transitional flows.

II. Transition Modeling

Laminar-to-turbulent flow transition modeling is one of the key factors in evaluating the CFD-based drag prediction using Reynolds-averaged Navier–Stokes (RANS) equations for external flow. Failing to accurately account for flow transition can result in wrong trend and value of all flow variables. This is due to the large discrepancy particularly in shear stress between the laminar and the turbulent regions. The flow behavior in these two zones differs significantly and thus all other flow variables. Add to this the fact that the transition zone might extend over a significant part of the airfoil surface. Thus, in cases where the laminar zone occupies a relatively large portion of the airfoil surface, neglecting its effect by assuming fully turbulent flow over the entire airfoil will result in numerically computed flow properties that can be significantly different from the actual values. This will lead to an inaccurate evaluation of the viscous properties in the boundary layer, and consequently an inaccurate drag prediction, and the value and position of $C_{L\max}$ (stall).

In a typical flow simulation using RANS solver coupled with a one- or two-equation turbulence model, the effective viscosity μ_{eff} is computed as

$$\mu_{\text{eff}} = \mu_L + \mu_t \tag{1}$$

where μ_L and μ_t are the laminar and turbulent viscosity, respectively. One of the methods of introducing transition in a fully turbulent boundary layer is by multiplying the turbulent viscosity by an intermittency function. Then the modified effective viscosity is equal to

$$\mu_{\text{eff}} = \mu_L + (\Gamma \times \mu_t) \tag{2}$$

Thus for $\Gamma = 0$, the boundary layer is fully laminar and for $\Gamma = 1$, the boundary layer is fully turbulent. For any value in between zero and one, the flow is in the transition region.

A. Transition Onset

For about a century, a large number of studies focused on predicting the transition criteria. However, until today, a complete understanding of this phenomenon and what physically is happening in the transition region have not been fully understood. Transition analysis is divided into two tasks; the first one is the transition onset prediction. Several analyses have been carried out to accurately predict the transition onset, which is the point where the disturbances in the laminar flow accumulate to a certain degree such that turbulent spots start to form and grow in the boundary layer. Studies concerning the prediction of transition onset can be classified in the following manner: by using empirical correlations, direct numerical simulations (DNS) by solving the unsteady Navier–Stokes equations, using the linear stability equations (LSE), or the parabolized stability equations (PSE). Although it has been proven that direct numerical simulation can predict the transition onset for simple flows, the large computer requirements and the difficulty that it encounters in the case of complex bodies makes it a hard choice to be implemented in engineering applications in the near future [3,4]. Regarding the PSE method, the concept is still new and its direct application into engineering is still far from realized [3]. On the other hand, a lot of effort has been put in the development of empirical correlations that would represent the experimental data about transition that have been collected. This could be due to the fact, that although theoretical analysis of transition is still not fully understood, the solution of such methods is elaborate and involves complicated mathematical methods. However, most of the empirical methods are based on incompressible two-dimensional flows. To name some, there are the methods of Michel (1951), Granville (1953), Smith and Gamberoni (1956), Van Ingen (1956), Crabtree (1958), and Van Driest and Blumer (1963) [5,6]. Of those that are widely recognized for their accuracy and ease of implementation in engineering applications are Michel's and Granville's methods [5]. Michel based his method on relating the transition momentum thickness Reynolds number $Re_{\theta,\text{tr}}$ to the local distance Reynolds number Re_x through a single curve that matches fairly well the experimental data for two-dimensional airfoils in incompressible flow for the following range of Reynolds numbers: $0.4 \times 10^6 < Re_x < 7 \times 10^6$. Later Cebeci and Smith [5], in accordance with Michel's method, suggested a similar curve that is compatible with the e^9 method and which is applicable for attached flows on airfoils for chord Reynolds numbers greater than two million [5,6]. On the other hand, Granville [5,6] has correlated the value of $Re_{\theta,\text{tr}} - Re_{\theta,xi}$ to the mean Pohlhausen parameter λ_m through a single curve. Here, $Re_{\theta,xi}$ is the Reynolds number based on the momentum thickness at the point of instability to Tollmien–Schlichting waves.

The linear stability equations analysis is based on the study of the disturbances that occur in the laminar boundary layer flow. By analyzing the behavior and stability of these waves (disturbances), known as the Tollmien–Schlichting instabilities, transition onset is predicted. This is done by finding the solution of the wave equations known as the Orr–Sommerfeld equation. The eigenvalues of the Orr–Sommerfeld equation can be found after applying the corresponding boundary conditions, and thus the amplification rate α and frequency ω can be calculated. Then the e^n method can be used to predict the transition onset. The factor n is defined as the logarithm of the maximum amplification ratio (A/A_0) calculated using the parameters α and ω obtained from the solution of the Orr–Sommerfeld equation [3]. Drela and Giles [7] developed a semi-empirical model to predict the transition onset; this model is based on the Orr–Sommerfeld equation coupled with empirical correlations originally developed for two-dimensional steady incompressible flow.

B. Transition Extent

The other aspect of the transition analysis process is that of the transition extent. That is the zone over which the boundary layer undergoes a change from a fully laminar flow to a fully turbulent flow. Such a region starts at the transition onset location and ends at the point where the flow is 100% turbulent. The region can be represented quantitatively by using intermittency functions. Such functions are defined as the percentage of time at which the flow is turbulent. A wide range of intermittency functions have been developed. Those functions are classified under three types: the linear-combination type, the algebraic type, and the differential type functions [8]. In the case of the linear-combination and algebraic model, the intermittency distribution is needed as an input. For the case of a differential model, the RANS equations of motion are solved with one- or two-equation turbulence closures. Narasimha has performed a detailed survey of the different transition models that have been proposed [8].

Dhawan and Narasimha [8,9] have correlated the experimental data and proposed a generalized distribution function across the transition region. Such a function, which is developed for two-dimensional incompressible flow over a flat plate, could be based on the hypothesis of concentrated breakdown. Chen and Thyson [10] based their work on Emmons' spot theory for predicting the transition and they have suggested an intermittency function to achieve a smooth transition from laminar into turbulent flow in the boundary layer. This function was defined for flows over blunt bodies, thus flow with pressure gradient, as opposed to the formula given by Dhawan and Narasimha which was based on flow over a flat plate [8,9]. Later Cebeci [11] added some modifications for the function so that it will include cases of two-dimensional low-Reynolds-number flows where laminar separation bubbles increase

in size and in occurrences. With those modifications in effect, the intermittency function covers data for Reynolds numbers that can be as low as 0.24 million.

Edwards et al. [12] have developed a one-equation turbulence/transition model that is based on both the Spalart–Allmaras one-equation turbulence model and a transition model that was developed by Warren and Hassan [13]. The intermittency function used by Edwards et al. [12] consists of two components. One is based on the work of Dhawan and Narasimha [8,9] and labeled as the surface-distance-dependent component. The other is a multidimensional component that is used to calculate the transition distribution normal to the surface. Then the two components are combined together to describe the transition zone distribution in the flow.

It is to be concluded that by using the empirical correlations developed to model both the onset and extent of transition, major time and effort can be saved in comparison with the percent accuracy to be gained by using more complex procedures.

III. Developed Transition Model

After reviewing the different procedures and methods developed to predict transition, let us make the following observations. First, to correctly predict the drag coefficient, the chosen method should be able to predict rather accurately the transition onset as well as the intermittency function that would represent the transition zone. While trying to achieve such an objective, the simplicity and ease of implementing such a procedure in a CFD flow simulation was to be taken into consideration. Moreover, the computing resources required to run the model should be a small fraction of that required to solve the RANS equations.

Thus the first task would be to predict the transition onset, and then a distribution function that would describe the transition zone is computed. The next step is to implement such a procedure in a turbulence model to calculate the turbulent viscosity and thus the different viscous flow parameters.

A. Transition Onset Prediction

To predict the transition onset location, the correlation derived by Cebeci and Smith [5] which is based on Michel's method is used. Cebeci and Smith suggest that the following correlation, which is compatible with the e^9 method, gives more accurate results than the one given originally by Michel [5,6]:

$$Re_\theta \approx 1.174\left[1 + \frac{22,400}{Re_x}\right]Re_x^{0.46} \qquad 0.1 \times 10^6 \le Re_x \le 40 \times 10^6 \tag{3}$$

Equation (3) is derived for attached flows on airfoils for chord Reynolds numbers greater than 2 million and it is based on incompressible fluid flow properties [5]. The momentum thickness is calculated using Thwaites method [14], which can predict $\theta(x)$ with an accuracy of $\pm 3\%$ for most types of incompressible laminar boundary layer flows [15]. The velocity at the boundary-layer edge is approximated with the inviscid flow velocity along the airfoil, which is computed by solving the Euler equations using Fluent. (The angle of attack used in the inviscid flow simulations was adjusted by 0.5–1.5 deg so as to match the position of the stagnation point observed in the turbulent flow calculations.) That velocity is also needed to compute the momentum thickness which is then used to find the transition onset and to evaluate the intermittency function later on.

B. Transition Extent Prediction

Modeling the transition extent is done by using an intermittency function that will divide the flow into three zones: the laminar zone with a corresponding intermittency function value of zero, the fully turbulent zone with a value of one, and the transition zone that will have a value that varies between zero at the beginning of transition and one where the flow becomes fully turbulent. The intermittency function used in the current work is a combination of two components, a surface-distance-dependent one and a normal-distance-dependent one. The two components are blended together through the following equation:

$$\Gamma(x, y) = 1 + \Gamma_b[\Gamma_x - 1] \tag{4}$$

To evaluate Γ_x, the function developed by Chen and Thyson [10] was used, taking into account the modifications added later on by Cebeci [11]. This modification was introduced by Cebeci to cover a wider range of Reynolds numbers; he did not provide any explanation for its origin other than the fact that it matches the experimental data better. Thus the equations used to compute Γ_x is defined as [10]

$$\Gamma_x = 1 - \exp\left[-G \times (x - x_t)\int_{x_{\text{tr}}}^{x} \frac{\mathrm{d}x}{u_e}\right] \tag{5}$$

where the factor G is given as

$$G = \frac{3}{C^2}\frac{u_e^3}{\nu^2}Re_{x,\text{tr}}^{-1.34} \tag{6}$$

and the parameter C is replaced by the term suggested by Cebeci [11]:

$$C^2 = 213(\log Re_{x,\text{tr}} - 4.7323) \tag{7}$$

where u_e is approximated by the inviscid velocity values as discussed in Sec. III.A.

The normal-distance-dependent term is evaluated based on the work of Edwards et al. [12]. Thus the equations used in the current model are

$$\Gamma_b(x, y) = \tanh(\eta^2) \tag{8}$$

where η is defined as

$$\eta = \frac{\max[0, \max(t_1, t_2) - t_\infty]}{t_3 + t_\infty} \tag{9}$$

The terms used in evaluating η are defined as

$$t_1 = \frac{500\nu}{d^2} \qquad t_2 = \frac{\sqrt{(\nu + \nu_t)\Omega}}{C_\mu^{3/2} d} \qquad t_3 = \sqrt{C_\mu}\Omega$$
$$t_\infty \approx 1 \times 10^{-5}\frac{U_\infty^2}{\nu_\infty} \tag{10}$$

The values of C_μ and t_∞ have been modified so as to match the CFD discretization method used in Fluent.

The transition model is then implemented into the flow solver, Fluent, where the RANS equations are solved with the Spalart–Allmaras turbulence model and the intermittency function $\Gamma(x, y)$ is introduced using the user-defined function feature that is available in Fluent. This function gives access to different variables in the flow solver and thus allows for modifying them [16]. The turbulent viscosity μ_t, computed using the fully turbulent Spalart–Allmaras turbulence model, is multiplied by $\Gamma(x, y)$ to reflect the introduction of the laminar and the transition zones into the fully turbulent boundary layer. Thus the modified effective viscosity μ_{eff} is computed as

$$\mu_{\text{eff}} = \mu_L + \Gamma \times \mu_t \tag{11}$$

IV. Flow Solver

Fluent is a commercial CFD software that solves the flow governing equations using a cell-centered control-volume space discretization method. In the present work, the flow equations are solved using an implicit coupled solver and a second-order upwind scheme is used to model artificial viscosity [17].

The system of equations that govern the fluid flow in the computational domain can be written for a control volume V enclosed by surface area A in the following format:

$$\frac{\partial}{\partial t}\int_V \boldsymbol{W}\,\mathrm{d}V + \oint [\boldsymbol{F}-\boldsymbol{G}]\cdot \mathrm{d}A = \int_V \boldsymbol{H}\,\mathrm{d}V \tag{12}$$

where the vectors $\boldsymbol{W}$, $\boldsymbol{F}$, and $\boldsymbol{G}$ are defined as

$$\boldsymbol{W} = \begin{pmatrix} \rho \\ \rho u \\ \rho v \\ \rho w \\ \rho E \end{pmatrix}, \qquad \boldsymbol{F} = \begin{pmatrix} \rho v \\ \rho v u + p\hat{i} \\ \rho v v + p\hat{j} \\ \rho v w + p\hat{k} \\ \rho v E + p v \end{pmatrix}, \qquad \boldsymbol{G} = \begin{pmatrix} 0 \\ \tau_{xi} \\ \tau_{yi} \\ \tau_{zi} \\ \tau_{ij} v_j + q \end{pmatrix} \tag{13}$$

and the vector $\boldsymbol{H}$ contains source terms such as body forces and energy sources. Here ρ, v, E, and p are the density, velocity, total energy per unit mass, and pressure, respectively. The viscous stress tensor is τ, and q is the heat flux. For low-Mach-number flows, the governing equations [Eq. (12)] are locally preconditioned to improve the convergence rate [17].

When it comes to modeling turbulence, it is impossible to assign a specific turbulence model as the one suitable for all kinds of flow problems. Thus to choose a specific turbulence model, a full understanding of the various models available with their potentials and limitations is essential. Also the flow physics to be covered should be investigated. The Spalart–Allmaras model is a one-equation turbulence model that solves a transport equation for the turbulent (eddy) viscosity. It was based on empiricism and arguments of dimensional analysis, Galilean invariance, and selective dependence on the molecular viscosity. It was developed specifically for aerospace applications involving wall-bounded flows and it gives good results for boundary layers with adverse pressure gradients [18]. Even though the original model developed by Spalart and Allmaras included transition terms where the transition onset has to be specified by the user, the model implemented into Fluent is fully turbulent [19]. To capture the laminar sublayer and the turbulent properties calculated by the Spalart–Allmaras model, a mesh that complies with the guidelines suggested by Fluent documentation should be used. These recommendations can be summed up as follows [19]:

1) To resolve the laminar sublayer, y^+ at the wall-adjacent cell should be on the order of $y^+ = 1$. However, a higher y^+ is acceptable as long as it is well inside the viscous sublayer ($y^+ < 4$–5).

2) At least 10 cells should be included within the viscosity-affected near-wall region to be able to resolve the mean velocity and turbulent quantities in that region.

V. Results

To assess the accuracy of the flow solver (Fluent) and to verify the effectiveness of the transition model, flow simulations were carried out for three well-documented experimental cases: a NACA0012 airfoil, a single-element airfoil [NLF(1)-0416], and a two-element airfoil (NLR-7301 with a trailing-edge flap). The results obtained with the new transition model were compared with experimental data and were also compared with those obtained with the fully turbulent flow simulations.

A. Accuracy Assessment of the CFD Solver Fluent

The accuracy of the CFD solver is first assessed for a NACA0012 with fully turbulent flow conditions, and is compared with experimental results. The assessment included the mesh type, the turbulence model, and the results sensitivity to y^+. A hybrid mesh, similar to the one shown in Fig. 1, was found to provide better resolution in the boundary layer (see Fig. 2). The fully turbulent Spalart–Allmaras model provided results for C_D and C_L more accurate than those given by the standard or the renormalization group (RNG) k–ε models, available in Fluent (see Fig. 3). As for the results sensitivity to the y^+, it was found that a value of y^+ average of one (which corresponds to $y/c \sim 5 \times 10^{-5}$) can be used to give a mesh independent solution (see Fig. 4).

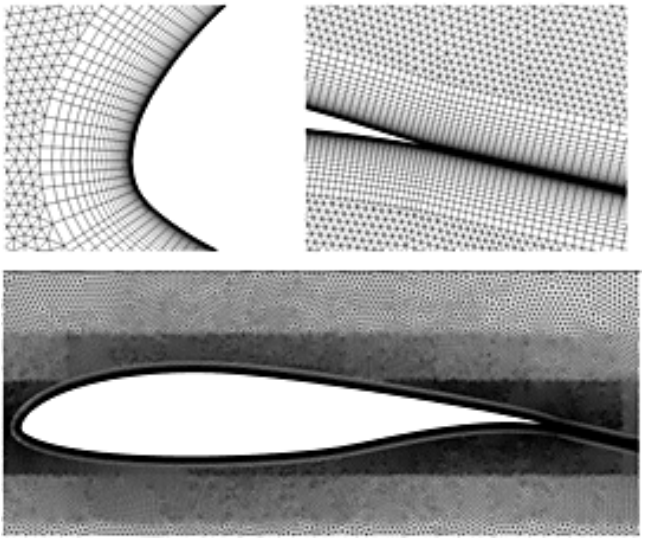

Fig. 1 Hybrid mesh over a NLF(1)-0416 airfoil.

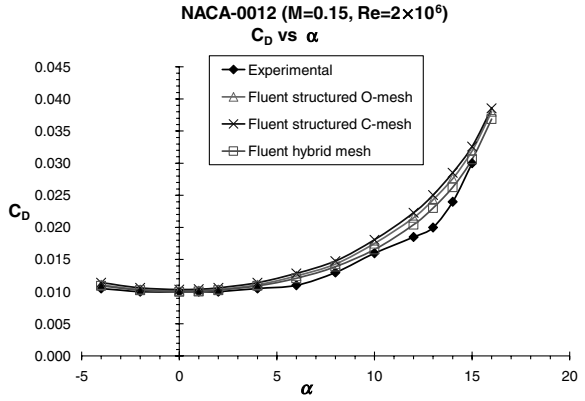

Fig. 2 Drag coefficient comparison between experimental and numerical data on three different meshes.

Based on this assessment, the following values and choice of parameters were used in obtaining the results presented in this section. The computational domain extends 30–50 chords away from the airfoil, and a hybrid mesh was constructed using Gambit. The far-field boundary conditions follow from the Riemann invariants (available in Fluent) [20]. A structured C-mesh, shown in Fig. 1, is built around the airfoil so as to control y^+ and the mesh stretching near the airfoil surface, and it extends for about 25% of the chord length at the trailing edge to capture the boundary layer and the wake. The distance of the first cell adjacent to the airfoil surface was taken

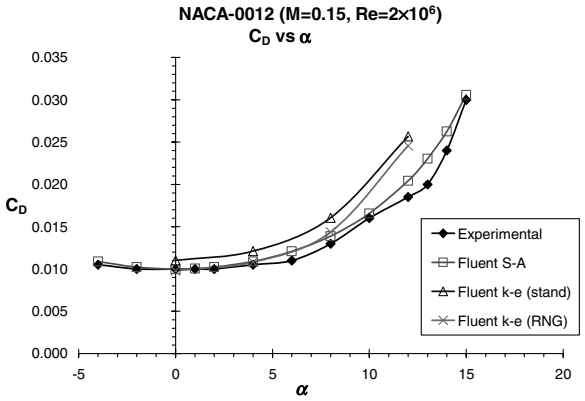

Fig. 3 Drag coefficient comparison between experimental and numerical data for different turbulence models.

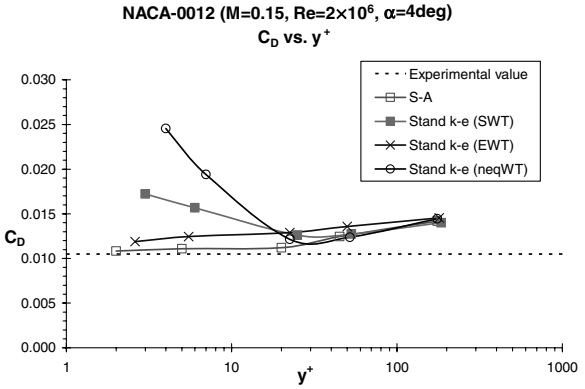

Fig. 4 Drag coefficient variation with respect to y^+ values for different wall treatment functions.

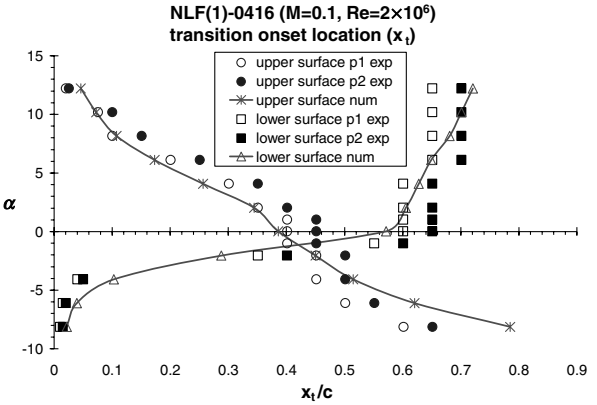

Fig. 5 Model validation of the transition onset.

to be 10^{-5} chord with the boundary layer structured mesh stretching for 35 cells in the direction normal to the airfoil surface. This ensured an average y^+ value that is about one, which is recommended by Fluent [19]. As for the grid distribution in the trailing-edge region, dx (dy) start at 10^{-4} (10^{-5}) at the trailing edge and gradually increases in the streamwise (normal) direction away from the trailing edge. The authors found that this resolution was sufficient. The remaining part of the computational domain is filled with unstructured triangular mesh (see Fig. 1). Convergence is measured by the L_2 norm on the residual of any of the governing equations at convergence; this value varies between 10^{-10} for low angles-of-attack cases and 10^{-5} for near-stall angles of attack. These choices were used in all of the results presented hereafter. For the NLF(1)-0416 and the NLR-7301 with a trailing-edge flap, relevant numerical details are given later. More information on the numerical accuracy can also be found in Basha [21].

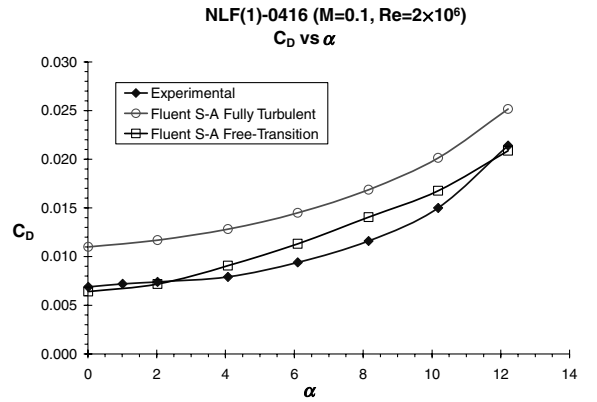

Fig. 6 Drag coefficient comparison between experimental and numerical results (uncertainty in experimental drag coefficient is 2%).

B. NLF(1)-0416 Airfoil

The NLF(1)-0416 is a natural-laminar-flow airfoil designed for use in light, single-engine, general aviation airplanes. It was developed by D. Somers at the NASA Langley Research Center for the purpose of obtaining an airfoil with a low cruise drag coefficient while maintaining a high maximum lift [22]. Numerical simulations were carried out on this airfoil using Fluent as the flow solver and the Spalart–Allmaras turbulence model with and without the transition model. The fully turbulent SA version used by Fluent is referred to as the fully turbulent model; the modified SA version, in which the free-transition model is implemented, is referred to as the free-transition model. Table 1 gives a summary of both experimental freestream conditions available and the numerical freestream conditions used in simulations. As for the grid, the number of nodes used to define the airfoil surface is 400, clustered near the leading and trailing edges to capture the flow behavior there. The whole mesh is composed of 157,250 cells that correspond to 92,173 nodes.

The numerical simulations presented in this section correspond to the following freestream conditions: Mach number $M_\infty = 0.1$, Reynolds number $Re_c = 2 \times 10^6$, and a range of angles of attack varying between 0 and 16 deg. The data obtained from the converged solutions were compiled and were used in producing the plots shown later. Figure 5 compares the transition onset predicted by the developed transition model with that obtained from the experimental data for different angles of attack. The transition onset is captured experimentally by using microphone measurements. Such a method is based on the concept that the laminar flow is silent, whereas a turbulent flow is noisy. Because the microphone is connected to individual orifices on the model, the onset location can only be determined as the region between two adjacent orifices [22]; this region is delimited by the open and closed symbols shown in Fig. 5. That figure also shows that the transition onset on both sides of the airfoil is changing in the same direction as that of the stagnation point so that when, e.g., the angle of attack is increased, the transition onset location moves forward on the upper surface and backward on lower surface of the airfoil. Such a behavior is in accordance with the one observed experimentally and expected physically. Quantitatively, the predicted transition onset is in the vicinity of the ranges given by the experimental data for a large range of angles of attack.

Figures 6 and 7 compare the variation of drag and lift coefficients with angle of attack α for three sets of data; one set is given experimentally [22] and the other two sets are obtained numerically by using the fully turbulent and the free-transition models. Examining the drag coefficient (Fig. 6), the improvement achieved in numerical drag computations by switching from a fully turbulent SA turbulence model to the developed free-transition one is quite clear. For zero angle of attack, the experimental drag coefficient is 69 drag

Table 1 Experimental and numerical freestream flow conditions for the NLF(1)-0416 case

	Mach number	Reynolds number	Angle of attack	Transition conditions
Experimental data	0.1–0.4	1–9 million	−16–17 deg	free transition[a]
Numerical data case 1	0.1	2 million	−16–16 deg	a) fully turbulent model b) free-transition model
Numerical data case 2	0.1	4 million	0–16 deg	a) fully turbulent model b) free-transition model

[a]Experimental data are available only for the following conditions: $M = 0.1$ and $Re = 1$–4 million.

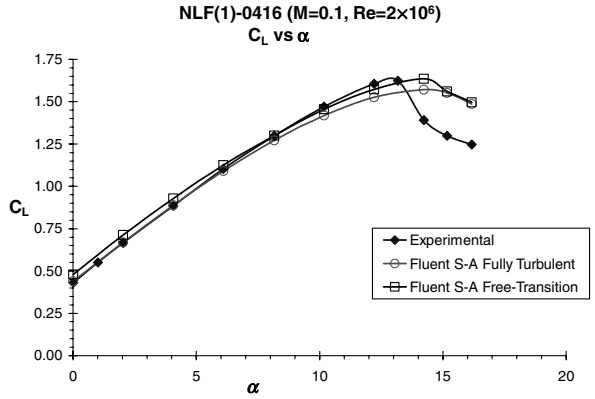

Fig. 7 Lift coefficient comparison between experimental and numerical results.

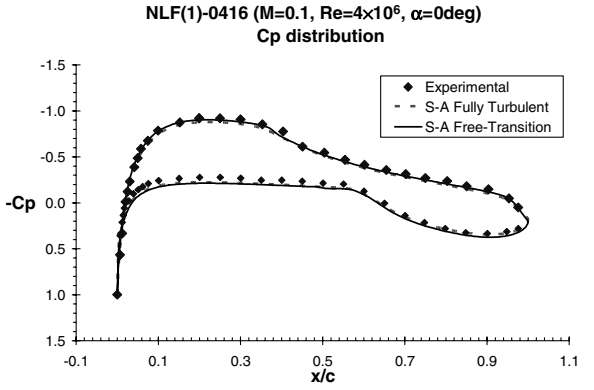

Fig. 9 Pressure coefficient comparison between experimental and numerical results.

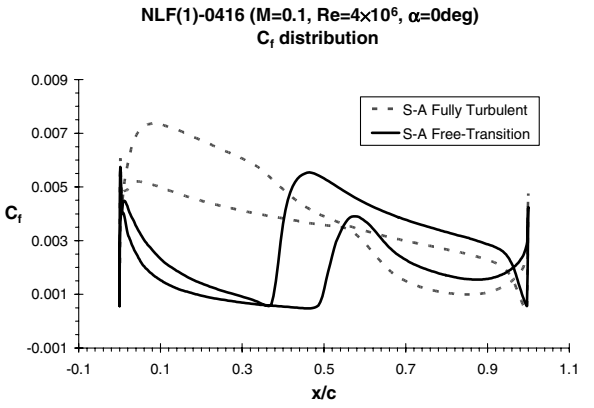

Fig. 10 Skin-friction coefficient comparison between numerical results.

counts (0.0069) whereas the value predicted using the fully turbulent model is 110 drag counts (0.011) with a variation from the experimental value equal to 41 drag counts. On the other hand, the values predicted using the free-transition model is equal to 64 drag counts with a variation from the experimental value equal to 5 drag counts. For angles of attack between 4 and 10 deg, the difference in drag coefficients given experimentally and those obtained using the fully turbulent model is on the average 50 drag counts, whereas the difference between the experimental values and those obtained using the free-transition model is on the average of 18 drag counts. And so, at angle of attack of 12 deg, where the experimental drag coefficient is equal to 214 drag counts, the difference in the value predicted by the fully turbulent model and the one given experimentally is equal to 37.5 drag counts, whereas it is about 5 drag counts for the free-transition model case.

As for the lift coefficient (Fig. 7), the curves can be divided into two sections: one corresponding to low values of angles of attack where $\alpha \leq 8$ deg and another one that corresponds to high values of angles of attack where $\alpha \geq 8$ deg. For the first section, the free-transition model overpredicts the lift with a maximum difference of 0.049 at zero angle of attack and an average difference equal to 0.032, whereas the difference between the experimental values and those predicted using the fully turbulent model is less than 0.01. However, for angles of attack higher than 8 deg the values predicted using the free-transition model are closer to the experimental data with a difference equal to 0.033 at an angle of attack equal to 12.2 deg. Finally, the location of $C_{L,\max}$ predicted numerically is delayed by about 1 deg for both models.

Figure 8 represents the polar drag plot for the current case ($M_\infty = 0.1,\ Re_c = 2 \times 10^6$) in which the experimental data are plotted as symbols, and the solid and dashed lines represent the free-transition and fully turbulent models, respectively. This figure highlights the improvement achieved when using the free-transition model where the corresponding curve is consistently closer to

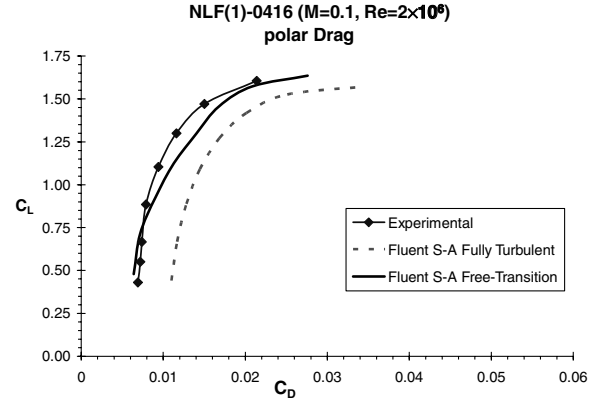

Fig. 8 Polar drag plot representing experimental and numerical data.

experimental data from the one obtained using the fully turbulent model.

Figures 9 and 10 represent the pressure coefficient and skin-friction coefficient for $M_\infty = 0.1$ and $Re = 4 \times 10^6$ at an angle of attack equal to 0 deg. In Fig. 9, the pressure coefficient is plotted for the experimental, the fully turbulent, and the free-transition cases. The Cp values obtained numerically, for both models, are in an excellent agreement with the experimental data. This confirms the fact that, for high-Reynolds-number attached flows, the pressure field and hence the lift are well predicted assuming inviscid flow (Euler equations) or even potential flow (viscous effects that set up the circulation around the airfoil are implicitly represented by applying the Kutta condition at the sharp trailing edge). As for the skin-friction coefficient distribution over the airfoils surface, and due to the absence of any experimental data, only numerical data obtained for the two models (fully turbulent and free-transition) are plotted in Fig. 10. The effect of introducing the free-transition model into the computation is evident. The skin-friction coefficient distribution in the leading part of the airfoil have changed to take into account the introduction of the laminar-transition zones by the free-transition model. The main conclusion that can be drawn from the Cp and C_f distributions is that, although the pressure field is almost unaffected by introducing the free-transition model, the skin-friction distribution reflects a strong dependency on transition. This emphasizes the fact that, although lift is strongly influenced by the inviscid flow behavior for attached flows, drag is controlled by the boundary-layer flow.

C. NLR-7301 Airfoil with a Trailing-Edge Flap

The next case considered is that of a two-element airfoil that is tested and well documented, the NLR-7301 airfoil with a trailing-edge flap. This case was identified as a good candidate to test the developed transition model. The geometry and experimental data

Table 2 Experimental and numerical freestream flow considerations for the NLR-7301 airfoil with a trailing-edge flap

	Experimental freestream flow	Numerical freestream flow
Mach number	0.185	0.185
Reynolds number	2.51×10^6	2.51×10^6
Angle of attack	0–16.1 deg (C_L) 6,10.1,13.1 deg (C_D)	0, 3, 6, 10.1, 13.1,14.1, 15.1 deg
Transition conditions	free transition	a) fully turbulent b) free transition

used for comparison are given in the AGARD AR-303 [23]. The experimental data are available for a freestream Mach number $M_\infty = 0.185$ and a Reynolds number $Re_c = 2.51 \times 10^6$. Also the geometric configuration used in this paper is that of a trailing-edge flap with a 2.6% gap. Although the surface pressure measurements are available for angles of attack between 0 and 16 deg at intervals of 1 deg, wake traverses and boundary layer measurements have been done at three angles of attack: 6, 10.1, and 13.1 deg. The error margin in the experimental data is given as ± 0.01 for the lift coefficient and $\pm 2\%$ for the drag coefficient [23]. The numerical simulations done in this work were carried out at selected angles of attack using the SA turbulence model with (free-transition) and without (fully turbulent) the transition model. Table 2 summarizes both the experimental and numerical data for the freestream conditions. The grid used to perform the numerical calculations is a hybrid mesh similar in structure and quality to the one used for the single-element airfoils. The number of nodes that define the airfoil surface is about 600 points clustered at the leading and trailing edges of the two elements. The first cell is at a distance of 10^{-5} chord from the wall and the mesh is composed of about 140,000 cells that correspond to about 81,000 nodes.

Figure 11 shows pressure coefficient distribution at two angles of attack: 6 and 13.1 deg. These plots show a good agreement between experimental results and the results obtained by the free-transition model. In Fig. 12, the transition onset predicted using the free-transition model is plotted alongside the experimental values for the three available angles of attack, namely 6, 10.1 and 13.1 deg. The main observation that can be pointed out by examining Fig. 12 is that the transition onset is well predicted on the main airfoil, although it is lagging the experimental values on the flap by almost one-third of the flap length, which is about 10% of the main element chord. This can be due to the fact that, although the flow is smooth and attached in the boundary layer at the leading edge of the main element, these conditions start to deteriorate downstream. Thus, for the case of the flap which is right behind the wake generated by the main element and is exposed to the jet coming from the pressure side through the gap, the assumptions under which the model was developed, namely incompressible attached flow, do not hold. Therefore, the free-transition model predictions are expected to be off. However, on the main airfoil, the predicted transition onset is in good agreement with the experimental data where the difference is about 4% of the chord on the lower side of the main element and less than 1% of the chord on the upper side.

The drag and lift coefficients obtained from the simulations are compiled together with the experimental data and are given in Figs. 13 and 14. Figure 13 shows a significant improvement in the drag values predicted using the free-transition model as opposed to

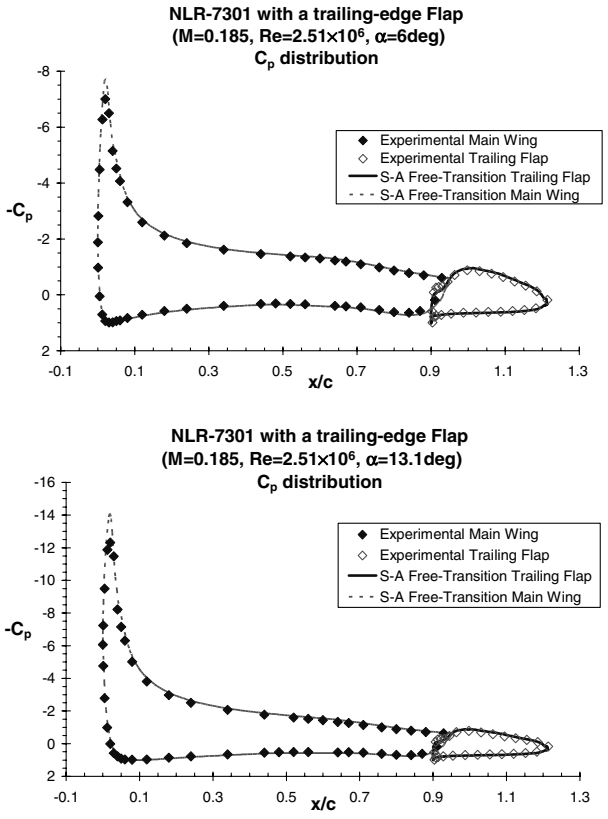

Fig. 11 Pressure coefficient comparison between experimental and numerical results.

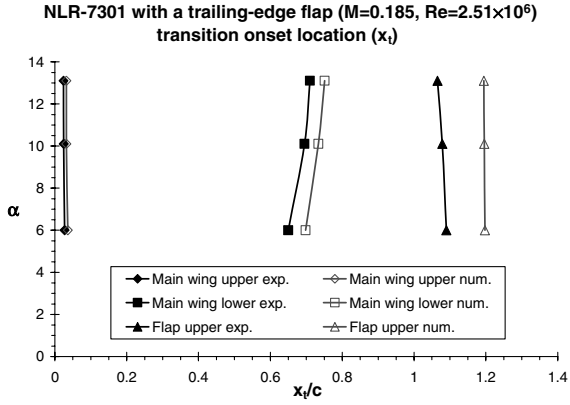

Fig. 12 Model validation of the transition onset.

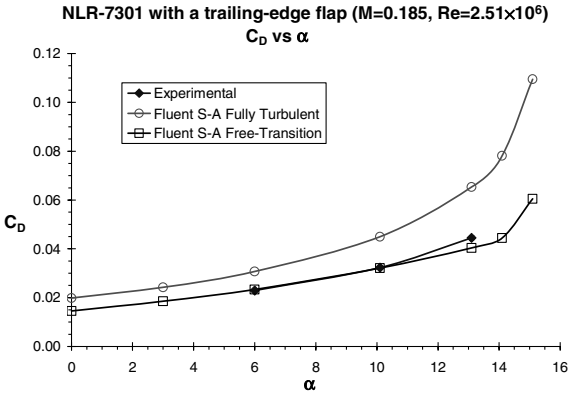

Fig. 13 Drag coefficient comparison between experimental and numerical results (experimental drag coefficient error margin is equal to ±2%).

Table 3 Difference in lift and drag coefficients between experimental and numerical results for the NLR-7301 airfoil with trailing-edge flap

Alpha	Exp.	Fully turbulent SA	Free-transition SA
	C_D, ±2% *error*	*Difference in* C_D *(compared with exp.)*	
6 deg	0.0229	78 drag count (34%)	5 drag count (2.1%)
10.1 deg	0.0323	127 drag count (40%)	2 drag count (0.6%)
13.1 deg	0.0445	208 drag count (47%)	41 drag count (9.3%)
	C_L ±0.01 *error*	*Difference in* C_L *(compared with exp.)*	
6 deg	2.416	0.0312 (1.3%)	0.1164 (5.1%)
10.1 deg	2.877	0.1495 (5.2%)	0.0362 (1.3%)
13.1 deg	3.141	0.3127 (10%)	0.0470 (1.5%)

those obtained using the fully turbulent model. For an angle of attack $\alpha = 6$ deg, the experimental drag coefficient is equal to 229 drag counts. The difference between the numerical value computed by the fully turbulent model and the experimental one is equal to 78 drag counts. This difference drops to 5 drag counts with the free-transition model. The results obtained for the other two angles of attack (10.1 and 13.1 deg) show the same behavior. Table 3 summarizes the difference in lift and drag coefficients, in reference to the experimental values, obtained using the two previously mentioned numerical models.

As for the lift analysis, Fig. 14 shows that the variation of the lift coefficient is also similar to that of the single-element airfoil. For $\alpha \leq 7$ deg, the free-transition model overpredicts the lift with an average difference of 0.138, whereas the difference between experimental values and those predicted using the fully turbulent model have an average difference of 0.015. For $\alpha > 7.1$ deg, the data predicted using the free-transition model are closer to the experimental data from the ones predicted using the fully turbulent model with an average difference equal to 0.05. On a positive note,

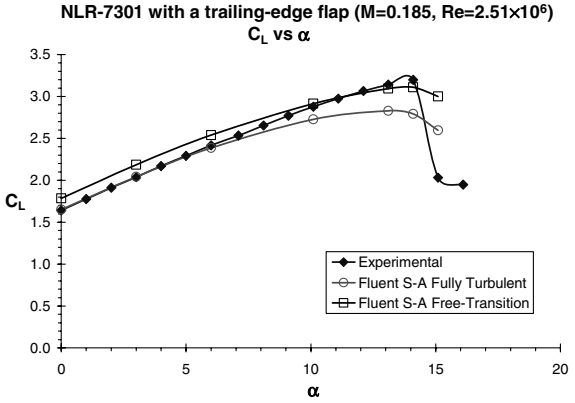

Fig. 14 Lift coefficient comparison between experimental and numerical results (uncertainty in experimental lift coefficient is equal to ±0.01).

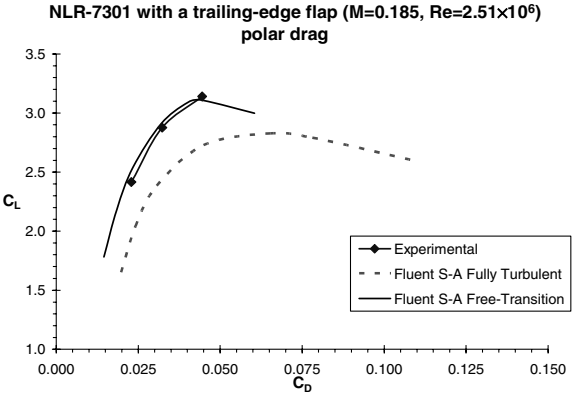

Fig. 15 Polar drag plot representing experimental and numerical data.

$C_{L,\max}$ predicted by the free-transition model is in good agreement with the experimental data, in both value and location.

Figure 15 represents the polar drag plot for the current case. The figure highlights the excellent agreement between experimental data and those obtained numerically using the free-transition model compared with the poor agreement between experimental data and those obtained using the fully turbulent model. This clearly demonstrates the value of the current transition model in accurately predicting the airfoil aerodynamic performance in terms of lift and drag.

VI. Conclusions

The objective of the current work was to develop a simple yet robust and accurate laminar-to-turbulent transition model that is capable of accurately predicting the drag in transitional flow over two-dimensional airfoils used typically in aerospace applications. This free-transition model predicts both the onset and the extent of transition; it is implemented into the fully turbulent SA turbulence model available in Fluent where the RANS equations are solved. The model was then used to simulate the flow over a wide range of angles of attack for two well-documented experimental cases: a single-element airfoil [NLF(1)-0416] and a two-element airfoil (NLR-7301 with a trailing-edge flap). In both cases, the drag values predicted using the developed free-transition model are closer to the experimental values when compared with those computed using the fully turbulent model. However, the accuracy in predicting the lift coefficient with the free-transition model deteriorates slightly at low angles of attack. Nonetheless, it can be concluded that the free-transition model, presented in this work, resulted in a significant improvement in drag prediction for airfoils in transitional flow.

References

[1] Van Dam, C. P., *Aircraft Design and the Importance of Drag Prediction*, VKI Lecture Series 2003-2: CFD-Based Aircraft Drag Prediction and Reduction, National Inst. of Aerospace, Hampton, VA, Nov. 2003.

[2] Van Dam, C. P., *Critical Factors in CFD-Based Aircraft Drag Prediction and Reduction*, VKI Lecture Series 2003-2: CFD-Based Aircraft Drag Prediction and Reduction, National Inst. of Aerospace, Hampton, VA, Nov. 2003.

[3] Cebeci, T., "Two-Dimensional Incompressible Flows: Transition Method," *Engineering Approach to the Calculations of Aerodynamic Flows*, 1st ed., Springer, New York, 1999, pp. 89–114.

[4] Reed, H. L., Haynes, T. S., and Saric, W. S., "Computational Fluid Dynamics Validation Issues in Transition Modeling," *AIAA Journal*, Vol. 36, No. 5, May 1998, pp. 742–751.

[5] Cebeci, T., and Smith, A. M. O., "CS Method for Turbulent Boundary Layers," *Analysis of Turbulent Boundary Layers*, 1st ed., Academic Press, New York, 1974, pp. 329–384.

[6] White, F. M., "Stability of Laminar Flows," *Viscous Fluid Flow*, 2nd ed., McGraw–Hill, New York, 1991, pp. 335–393.

[7] Drela, M., and Giles, M. B., "Viscous-Inviscid Analysis of Transonic and Low Reynolds Number Airfoils," *AIAA Journal*, Vol. 25, No. 10, Oct. 1987, pp. 1347–1355.

[8] Narasimha, R., "Modeling the Transitional Boundary Layer," Inst. for Computer Applications in Science and Engineering Rept. No. 90-90, Dec. 1990.

[9] Dhawan, S., and Narasimha, R., "Some Properties of Boundary Layer

Flow During the Transition from Laminar to Turbulent Motion," *Journal of Fluid Mechanics*, Vol. 3, Jan. 1958, pp. 418–436.
[10] Chen, K., and Thyson, N., "Extension of Emmons Spot Theory to Flows on Blunt Bodies," *AIAA Journal*, Vol. 9, No. 5, May 1971, pp. 821–825.
[11] Cebeci, T., "Essential Ingredients of a Method for Low Reynolds-Number Airfoils," *AIAA Journal*, Vol. 27, No. 12, Dec. 1989, pp. 1680–1688.
[12] Edwards, J. R., Roy, C. J., Blottner, F. G., and Hassan, H. A., "Development of a One-Equation Transition/Turbulence Model," *AIAA Journal*, Vol. 39, No. 9, Sept. 2001, pp. 1691–1698.
[13] Warren, E. S., and Hassan, H. A., "Transition Closure Model for Predicting Transition Onset," *Journal of Aircraft*, Vol. 35, No. 5, Sept.–Oct. 1998, pp. 769–775.
[14] Thwaites, B., "Approximate Calculations of the Laminar Boundary Layer," *Aeronautical Quarterly*, Vol. 1, Nov. 1949, pp. 245–280.
[15] White, F. M., "Laminar Boundary Layers," *Viscous Fluid Flow*, 2nd ed., McGraw–Hill, New York, 1991, pp. 218–334.
[16] Anon. "Ch.1: Overview," *Fluent 6.2 UDF Manual*, Fluent Lebanon, NH, Jan. 2005.
[17] Anon., "Ch.26: Using the Solver" *Fluent 6.2 User's Guide*," Fluent, Lebanon, NH, Jan. 2005.
[18] Spalart, P. R., and Allmaras, S. R., "One Equation Turbulence Model for Aerodynamic Flows," AIAA Paper 92-0439, Jan. 1992.
[19] Anon., Ch.11: Modeling Turbulence," *Fluent 6.2 User's Guide*, Fluent, Lebanon, NH, Jan. 2005.
[20] Anon., "Ch.7: Boundary Conditions," *Fluent 6.2 User's Guide*, Fluent, Lebanon, NH, Jan. 2005.
[21] Basha, W., "Accurate Drag Prediction for Transitional External Flow Over Airfoils," M.Sc. Thesis, Concordia Univ., Dept. of Mechanical and Industrial Engineering, Montreal, Canada, 2006.
[22] Somers, D. M., "Design and Experimental Results for a Natural-Laminar-Flow Airfoil for General Aviation Applications," NASA TP 1861, June 1981.
[23] Van Den Berg, B., and Gooden, J. H. M., "Low-Speed Surface Pressure and Boundary Layer Measurement Data for the NLR-7301 Airfoil Section with Trailing Edge Flap," *Selection of Experimental Test Cases for the Validation of CFD Codes*, AGARD AR-303, Aug. 1994.